Available online at www.sciencedirect.com
ScienceDirect
ELSEVIER
International Journal of Thermal Sciences 47 (2008) 486–494
International Journal of Thermal Sciences
www.elsevier.com/locate/ijts

Performance investigation of thermoelectrics with an external spacer inserted in serious

Jake Kim [a], Yong Tae Kang [b,*], Sang Nyung Kim [b], Joo Ho Hwang [b], Soon Geul Lee [b], Hiki Hong [b], Moo-Geun Kim [c]

[a] *CAE Team, Corporate R&D Center, Samsung SDI Co. Ltd., Kyung-Gi, 449-577, South Korea*
[b] *School of Mechanical and Industrial Systems Engineering, Kyung Hee University, Kyung-Gi, 449-701, South Korea*
[c] *School of Mechanical and Automotive Engineering, Inje University, Kyongnam, 621-749, South Korea*

Received 6 October 2006; received in revised form 25 March 2007; accepted 25 March 2007

Available online 23 May 2007

Abstract

This study consists of two parts: mathematical modeling for the start-up period (transient system) and an optimum design analysis of a thermoelectric cooler (TEC). In the mathematical modeling for the transient system, a dimensionless time to reach the steady state is determined, which can be practically adopted to reduce the start-up period during the operation of a thermoelectric module (TEM). The objectives of the optimum design analysis are to investigate the effect of key parameters characterizing the TEC on the coefficient of performance (*COP*) and to determine the optimal conditions for the TEC design. It is found that the *COP* increases up to 44% with an increase of the ratio of heat transfer area of the insulator to that of the TEM, γ. For micro-TEC, the *COP* is significantly affected by the TEM depth and spacer. Especially in the case of TEM depth of 100 µm, the *COP* is enhanced up to 110% at an optimal spacer depth ratio ($\varepsilon - 1$) of 10. The results show that the effect of figure of merit Zm ($= S^2/RK_{TE}$) on the *COP* appears differently according to the combination of thermal conductance K_{TE}, electric resistance R and Seebeck constant S of the TEM. It reveals that when a new thermoelectric material is developed, the optimal combination among K_{TE}, R, and S as well as Zm should be considered simultaneously.
© 2007 Elsevier Masson SAS. All rights reserved.

Keywords: Thermoelectric cooler; Thermoelectric module; Coefficient of performance; Figure of merit

1. Introduction

Thermoelectric coolers (TEC) with thermoelectric modules (TEM) have been widely employed in many areas demanding accurate control by micro-sized cooling devices such as military, aerospace, and medical applications. The usage of this device is expanded to living system appliance, i.e. portable refrigerator and cooling cap due to the increasing demand of high quality of human life [1–3]. The research on the TEC can be divided largely into two fields; the development of thermoelectric materials [4–6] and the heat transfer enhancement of TEC with TEM [7–10].

In the field of material development, the improvement of the figure of merit, Zm ($= S^2/RK_{TE}$) has been considered as a key factor to measure the thermoelectricity of materials. Recently the thermoelectric materials with the dimensionless figure of merit, ZmT of 0.6 are developed by Toprak [6]. In the field of heat transfer enhancement, Yamanashi [7] investigated the optimum design conditions using the analysis of the heat balance in TEM and TEC respectively. Because he introduced the concept of heat load instead of thermal resistance in hot and cold sides, the effect of TEC geometries such as heat transfer area of TEC and the depth of TEM on the performance of TEC could not be analyzed. Min and Rowe [8] studied the effects of the electric and thermal contact resistance, thermal bypass, and radiation on the performance in the micro TEC system. They reported that the coefficient of performance (*COP*) became the maximum at TEM depth of 500 µm. Huang et al. [9] obtained the experimen-

* Corresponding author. Tel.: +82 31 201 2990; fax: +82 31 202 8106.
E-mail address: ytkang@khu.ac.kr (Y.T. Kang).

1290-0729/$ – see front matter © 2007 Elsevier Masson SAS. All rights reserved.
doi:10.1016/j.ijthermalsci.2007.03.017

Nomenclature

a, b, c, d	coefficients in equations	
A, B, C, D, E, F	coefficients in equations	
A	area of heat transfer	m^2
A_i	heat transfer area of insulator	m^2
A_{TE}	heat transfer area of thermoelectric module	m^2
COP	coefficient of performance, Q_c/P	
d	TEM depth	m
I	current	A
k	thermal conductivity	W/mK
K_{TE}	thermal conductance ($= k_{TE} \cdot l_{TE}$)	W/K
L	heat load	W/K
l_{TE}	characteristic length of thermoelectric module	m
m	dummy variable in Eq. (13)	
P	electric power	W
R	electric resistance	Ω
q	heat flux	W/m^2
Q	heat	W
s	dummy variable in Eq. (8)	
S	Seebeck constant	V/K
t	time	s
T	temperature	K
z	dimensionless coordinate, Z/d	
Z	coordinate	m
Zm	figure of merit, S^2/RK_{TE}	K^{-1}

Greek symbols

α	thermal diffusivity	m^2/s
ε	depth ratio of insulator to TEM	
γ	area ratio, A_i/A_{TE}	
κ	dimensionless thermal diffusivity, α_i/α	
θ_c	dimensionless temperature in cold side, $\frac{T-T_{co}}{T_c-T_{co}}$	
θ_h	dimensionless temperature in hot side, $\frac{T-T_{ho}}{T_h-T_{ho}}$	
θ_i	dimensionless temperature in insulator, $\frac{T-T_{io}}{T_h-T_{io}}$	
θ_1	dimensionless temperature difference, $\frac{T_c-T_{co}}{T_h-T_{io}}$	
θ_2	dimensionless temperature difference, $\frac{T_{co}-T_{io}}{T_h-T_{io}}$	
σ	depth ratio of heat sink to TEM	
τ	dimensionless time, $\alpha t/d^2$	

Subscripts

c	cold side
co	surface of cold side
h	hot side
ho	surface of hot side
i	insulator
s	steady state
TE	thermoelectric module
ε	interface between insulator and cold side

tal correlations between the *COP* and the current I, and lately, Luo et al. [10] showed theoretically that there is an optimum value of heat transfer area for given conditions.

Most recently, Cheng and Shih [11] presented a design model based on genetic algorithm to maximize the cooling capacity and *COP* for two-stage thermoelectric coolers. Their model dealt with the temperature-dependent material properties and considered the effects of contact and spreading resistances. They proposed that the cooling capacity and the *COP* could be improved by properly tuning the design parameters. Yu et al. [12] also conducted thermodynamic modeling for a basic two-stage thermoelectric module, which contains one thermocouple in the second stage and several thermocouples in the first stage. They found that the cooling performance of the module could be improved by changing the junction temperature difference in the second stage, length and numbers of the thermocouples in the first stage. Chakraborty and Ng [13] presented a thermodynamic formation of temperature-entropy diagram for the transient operation of a pulsed thermoelectric cooler based on the Gibbs law. Pramanick and Das [14] carried out a control volume formulation of a cascaded thermoelectric element, and identified three important dimensionless parameters to designate poor Thomson effect; low thermal conductivity and low electrical resistivity of a good semiconductor or semimetal. Vikhor and Anatychuk [15] calculated optimal parameter values of BiTe-based materials for thermoelectric coolers with single-, double-, and three-segmented legs, and found that the use of more than two segments was not recommended owing to the parasitic effect of contact resistance between the segments.

Conventional TEC consists of insulator, spacer, TEM and two heat sinks. Generally, the area of heat sinks is made larger than that of TEM to enhance the heat transfer to the surroundings. This structure may cause the great heat loss from hot to cold side through the insulator in case of a micro-sized TEM depth. To reduce the heat loss, the spacer is inserted between heat sink and TEM. The spacer is made by the same material of heat sinks (aluminum) as usual.

This paper proposes a theoretical model for optimum design of not only the conventional TEM but also the micro-sized one. There is a start-up period before a system reaches to the steady state. This study consists of two parts: mathematical modeling for the start-up period (transient system) and steady analysis of TEC for optimum design. In the mathematical modeling for a transient system, a dimensionless time to reach the steady state is determined, which can be practically adopted to reduce the start-up period during the operation of TEM. The objective of the steady analysis is to theoretically investigate the effect of parameters such as heat transfer area, spacer depth, and thermoelectricities of TEM on the *COP* in TEC with a spacer for optimum design of a TEM.

2. Mathematical modeling for transient systems

Fig. 1 shows the schematic diagram of a TEC with two heat sinks and a spacer. The TEM as a heat pump has a depth d. The heat transfer areas of the heat sinks are the same and are larger

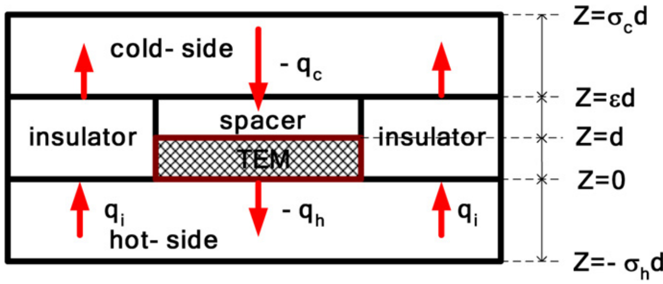

Fig. 1. Schematic diagram for the TEC with a spacer.

than that of the TEM. The insulator prohibits heat loss from the hot section the cold one. On the other hand, the spacer helps heat to transfer from the cold side to the TEM. In order to simplify the modeling, it is assumed that the contact resistances are neglected and the thermoelectric properties are independent of temperature [16]. Furthermore, a horizontal thermal resistance of heat sinks is neglected because the ratio of heat sink area to TEM area is sufficiently small. This approximation changes a multi-dimensional heat conduction into an one-dimensional one.

With the above assumptions, an unsteady, one-dimensional conduction in hot and cold side is governed identically by

$$\frac{\partial T}{\partial t} = \alpha \frac{\partial^2 T}{\partial Z^2} \tag{1}$$

with the following initial and boundary conditions of hot and cold sides.

(Hot side)

$$T = T_{ho}, \quad t = 0 \tag{2}$$

$$T = T_h, \quad Z = 0 \tag{3}$$

$$T = T_{ho}, \quad Z = -\sigma_h d \tag{4}$$

(Cold side)

$$T = T_{co}, \quad t = 0 \tag{5}$$

$$T = T_c, \quad Z = d \tag{6}$$

$$T = T_{co}, \quad Z = \sigma_c d \tag{7}$$

For an unsteady conduction system, the dimensionless solutions with the above equations are obtained by using the Laplace transformation method, respectively [17].

(Hot side)

$$\theta_h = \sum_{s=0}^{\infty} \left\{ \operatorname{erfc}\left(\frac{a_h(s,z)}{2\sqrt{\tau}}\right) - \operatorname{erfc}\left(\frac{b_h(s,z)}{2\sqrt{\tau}}\right) \right\} \tag{8}$$

(Cold side)

$$\theta_c = \sum_{s=0}^{\infty} \left\{ \operatorname{erfc}\left(\frac{a_c(s,z)}{2\sqrt{\tau}}\right) - \operatorname{erfc}\left(\frac{b_c(s,z)}{2\sqrt{\tau}}\right) \right\} \tag{9}$$

where

$$a_h(s,z) = 2\sigma_h s - z$$

$$b_h(s,z) = 2\sigma_h s + \sigma_h + z$$

$$a_c(s,z) = 2(\sigma_c - 1)s - 1 + z$$

$$b_c(s,z) = 2(\sigma_c - 1)s + 2\sigma_c - 1 - z$$

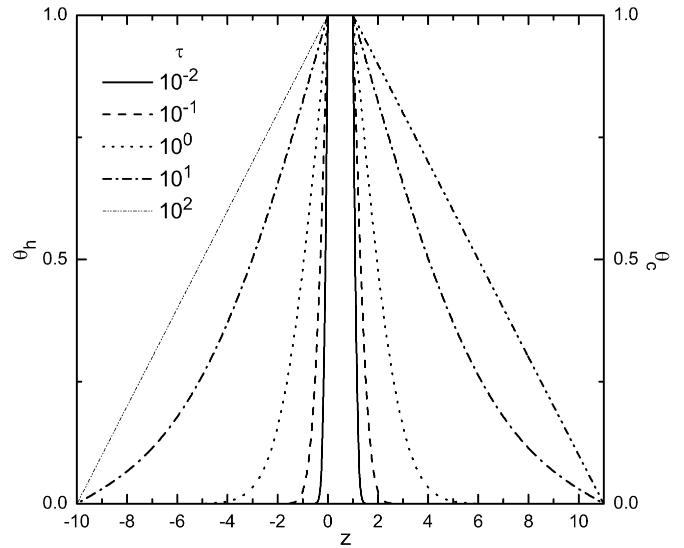

Fig. 2. Dimensionless temperature profiles in hot and cold sides for various dimensionless time.

In the present study, the TEM depth, d, instead of heat sink depths, $\sigma_h d$ or $\sigma_c d$ is chosen as the characteristic length scale factor in order to investigate the effect of TEM depth.

The temperature profiles in hot and cold sides are plotted in Fig. 2 based on Eqs. (8) and (9), respectively. It shows that dimensionless temperatures of the hot and cold side are symmetrical and conduction reaches the steady state at $\tau = 100$.

The conduction equation of dimensionless temperature in an insulator is expressed as follows

$$\frac{\partial \theta_i}{\partial \tau} = \kappa \frac{\partial^2 \theta_i}{\partial z^2} \tag{10}$$

The boundary conditions are obtained from Eqs. (8) and (9) respectively.

$$\theta_i = 1, \quad z = 0 \tag{11}$$

$$\theta_i = \theta_c(\varepsilon) + \theta_1 + \theta_2, \quad z = \varepsilon \tag{12}$$

where θ_1 and θ_2 represent dimensionless temperature differences of the cold side (see Nomenclature).

Using the Laplace transformation, the dimensionless temperature in the insulator is obtained as follows:

$$\begin{aligned}\theta_i = \sum_{s=0}^{\infty} \Bigg[\Bigg\{ &\operatorname{erfc}\left(\frac{a_0(s,z)}{2\sqrt{\tau}}\right) - \operatorname{erfc}\left(\frac{b_0(s,z)}{2\sqrt{\tau}}\right) \\ &- \theta_2\left(\operatorname{erfc}\left(\frac{a_1(s,z)}{2\sqrt{\tau}}\right) - \operatorname{erfc}\left(\frac{b_1(s,z)}{2\sqrt{\tau}}\right)\right)\Bigg\} \\ &+ \theta_1 \sum_{m=0}^{\infty} \Bigg\{ \operatorname{erfc}\left(\frac{c_1(m,s,z)}{2\sqrt{\tau}}\right) - \operatorname{erfc}\left(\frac{d_1(m,s,z)}{2\sqrt{\tau}}\right) \\ &- \theta_2\left(\operatorname{erfc}\left(\frac{c_2(m,s,z)}{2\sqrt{\tau}}\right) - \operatorname{erfc}\left(\frac{d_2(m,s,z)}{2\sqrt{\tau}}\right)\right)\Bigg\}\Bigg]\end{aligned} \tag{13}$$

where

$$a_0(s,z) = \frac{2\varepsilon}{\sqrt{\kappa}}s + \frac{z}{\sqrt{\kappa}}$$
$$b_0(s,z) = \frac{2\varepsilon}{\sqrt{\kappa}}s + \frac{2\varepsilon}{\sqrt{\kappa}} - \frac{z}{\sqrt{\kappa}}$$
$$a_1(s,z) = a_0(s,z) + \frac{\varepsilon}{\sqrt{\kappa}}$$
$$b_1(s,z) = b_0(s,z) - \frac{\varepsilon}{\sqrt{\kappa}}$$
$$c_0(m,s) = \frac{2\varepsilon}{\sqrt{\kappa}}m + 2(\sigma_c - 1)s + 2\sigma_c - \varepsilon + \frac{\varepsilon}{\sqrt{\kappa}} - 1$$
$$d_0(m,s) = \frac{2\varepsilon}{\sqrt{\kappa}}m + 2(\sigma_c - 1)s + \frac{\varepsilon}{\sqrt{\kappa}} + \varepsilon - 1$$
$$c_1(m,s,z) = c_0(m,s) + \frac{z}{\sqrt{\kappa}}$$
$$d_1(m,s,z) = d_0(m,s) + \frac{z}{\sqrt{\kappa}}$$
$$c_2(m,s,z) = c_0(m,s) - \frac{z}{\sqrt{\kappa}}$$
$$d_2(m,s,z) = d_0(m,s) - \frac{z}{\sqrt{\kappa}}$$

Now, assuming the hot and cold sides are in steady state while the insulator is in unsteady, the following solution is obtained.

$$\theta_i = \sum_{s=0}^{\infty}\left[\operatorname{erfc}\left(\frac{a_0(s,z)}{2\sqrt{\tau}}\right) - \operatorname{erfc}\left(\frac{b_0(z)}{2\sqrt{\tau}}\right) - \theta_\varepsilon\left\{\operatorname{erfc}\left(\frac{a_1(s,z)}{2\sqrt{\tau}}\right) - \operatorname{erfc}\left(\frac{b_1(s,z)}{2\sqrt{\tau}}\right)\right\}\right] \tag{14}$$

It can also be obtained by replacing θ_1 and θ_2 by zero and θ_ε in Eq. (13), respectively. Eq. (14) is plotted for various dimensionless times τ in Fig. 3. The results show that insulator reaches the steady state at $\tau = 10^5$ while heat sinks at $\tau = 10^2$.

Rearranging Eq. (14), the unsteady heat flux in the insulator is expressed as follows:

$$q_i = \frac{k_i}{d}(T_h - T_{io})\frac{1}{\sqrt{\pi\kappa\tau}}\sum_{s=0}^{\infty}\left[\left\{\exp\left(\frac{a_0(s,z)^2}{4\tau}\right) - \exp\left(\frac{b_0(s,z)^2}{4\tau}\right)\right\} - \theta_\varepsilon\left\{\exp\left(\frac{a_1(s,z)^2}{4\tau}\right) - \exp\left(\frac{b_1(s,z)^2}{4\tau}\right)\right\}\right] \tag{15}$$

As shown in Fig. 4, q_i decreases sharply for small τ depending on z and reaches a certain mean value at $\tau = 10^2$.

In order to investigate the effect of heat loss through the insulator with time, the mean heat flux at the insulator is defined as follow:

$$\bar{q}_i = \frac{\int_0^\varepsilon q_i\,\mathrm{d}z}{\int_0^\varepsilon \mathrm{d}z} \tag{16}$$

Because the temperature field is the potential of heat flux, q $(= -k\nabla T)$ the integration of q_i over the insulator changes to a simple form expressed by temperature differences.

$$\int_0^\varepsilon q_i\,\mathrm{d}z = -\frac{k_i}{d}(T_h - T_{io})\big[\theta_i(\varepsilon) - \theta_i(0)\big] = \frac{k_i}{d}(T_h - T_{\varepsilon d}) \tag{17}$$

Substituting Eq. (17) into Eq. (16) yields

$$\bar{q}_i = \frac{k_i}{\varepsilon d}(T_h - T_{\varepsilon d}) = q_{i,s} \tag{18}$$

It shows that $\bar{q}_i$ is the same as the heat flux at the steady conduction. According to Fig. 4, after $\tau = 10^2$, steady condition can be applicable to analysis of TEC for optimal design. Therefore, in the following section, steady analysis of TEC is carried out for optimum design.

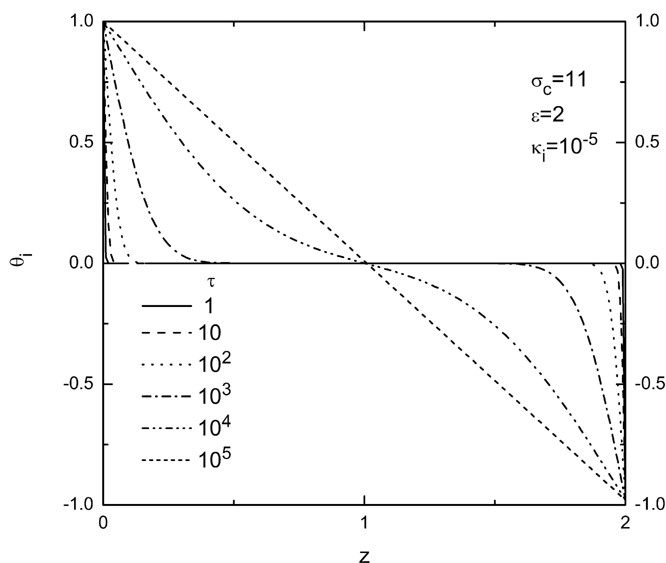

Fig. 3. Dimensionless temperature profiles in the insulator for various dimensionless time.

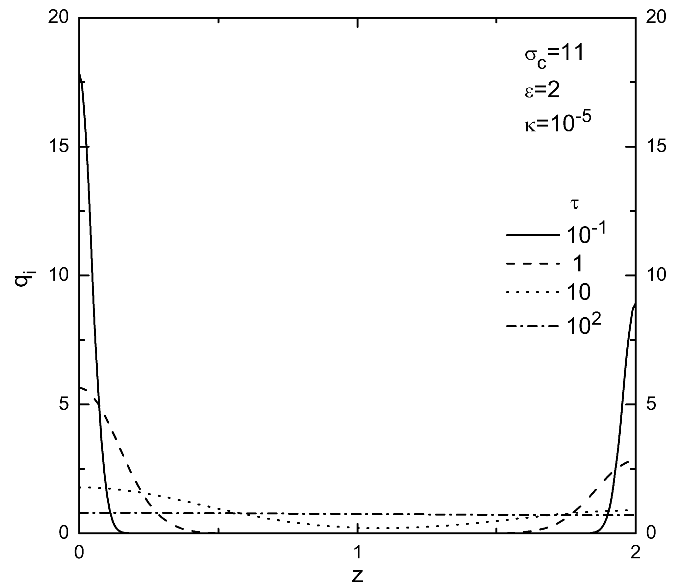

Fig. 4. The variation of unsteady heat flux in the insulator for various dimensionless time.

3. Optimal design analysis

After reaching the steady state, the heat transfer analysis is performed in order to find the optimal conditions for maximizing the *COP* of the convectional TEC. Considering heat loss through the insulator, heat balances with heat transfer area of heat sink in hot and cold sides are expressed, respectively, as follows:

$$Q_c = q_c A_{TE} - q_{i,s} A_i = (A_{TE} + A_i)\frac{k}{(\sigma_c - \varepsilon)d}(T_{co} - T_{\varepsilon d}) \tag{19}$$

$$Q_h = q_h A_{TE} - q_{i,s} A_i = (A_{TE} + A_i)\frac{k}{\sigma_h d}(T_h - T_{ho}) \tag{20}$$

In case of $A_i = 0$, $L_c = k/(\sigma_c - \varepsilon)d$, and $L_h = k/\sigma_h d$, Eqs. (19) and (20) are identical to Yamanashi's heat balance [7].

Energy balance at TEM is well known as follows [18,19]

$$q_c A_{TE} = SIT_c - \frac{I^2 R}{2} - K_{TE}(T_h - T_c) \tag{21}$$

$$q_h A_{TE} = SIT_h + \frac{I^2 R}{2} - K_{TE}(T_h - T_c) \tag{22}$$

Introducing Eq. (18) into Eqs. (19) and (20) yields

$$q_c A_{TE} = (A_{TE} + A_i)\frac{k}{(\sigma_c - \varepsilon)d}(T_{co} - T_{\varepsilon d}) + A_i \frac{k_i}{\varepsilon d}(T_h - T_{\varepsilon d}) \tag{23}$$

$$q_h A_{TE} = (A_{TE} + A_i)\frac{k}{\sigma_h d}(T_h - T_{ho}) + A_i \frac{k_i}{\varepsilon d}(T_h - T_{\varepsilon d}) \tag{24}$$

Eqs. (21)–(24) can be arranged as a 2×2 matrix form for T_c and T_h

$$\begin{pmatrix} A & B \\ C & D \end{pmatrix}\begin{pmatrix} T_c \\ T_h \end{pmatrix} = \begin{pmatrix} E \\ F \end{pmatrix} \tag{25}$$

where

$$A = A_i \frac{k}{\varepsilon d}\left(\frac{\varepsilon - 1}{\sigma_c - 1} - 1\right) - (A_{TE} + A_i)\frac{k}{(\sigma_c - \varepsilon)d} - (SI + K_{TE})$$

$$B = A_i \frac{k_i}{\varepsilon d} + K_{TE}$$

$$C = A_i \frac{k}{\varepsilon d}\left(\frac{\varepsilon - 1}{\sigma_c - 1} - 1\right) - K_{TE}$$

$$D = (A_{TE} + A_i)\frac{k}{\sigma_h d} + A_i \frac{k_i}{\varepsilon d} - (SI - K_{TE})$$

$$E = -\left\{\left[(A_{TE} + A_i)\frac{k}{(\sigma_c - \varepsilon)d} - A_i \frac{k_i}{\varepsilon d}\frac{\varepsilon - 1}{\sigma_c - 1}\right]T_{co} + \frac{I^2 R}{2}\right\}$$

$$F = (A_{TE} + A_i)\frac{k}{\varepsilon d}T_{ho} + A_i \frac{k_i}{\varepsilon d}\frac{\varepsilon - 1}{\sigma_c - 1}T_{co} + \frac{I^2 R}{2}$$

The solution is obtained by the method of linear algebra as follows.

$$\begin{pmatrix} T_c \\ T_h \end{pmatrix} = \frac{1}{AD - BC}\begin{pmatrix} DE - BF \\ AF - CE \end{pmatrix} \tag{26}$$

where $AD - BC \neq 0$.

The electric power P which is supplied to the TEM is expressed as follows:

$$P = q_h A_{TE} - q_c A_{TE} \tag{27}$$

The *COP* for the TEC is defined as

$$COP = \frac{Q_c}{P} \tag{28}$$

Combining Eqs. (19), (21), (22), (27), and (28), the *COP* is expressed as

$$COP = \frac{\frac{\sigma_h}{\sigma_c - \varepsilon}\frac{T_{co} - T_c}{T_h - T_{ho}}}{1 - \frac{\sigma_h}{\sigma_c - \varepsilon}\frac{T_{co} - T_c}{T_h - T_{ho}}} \tag{29}$$

From Eqs. (26) and (29), the effect of parameters, γ, d, σ_h, I, K_{TE}, R, S, and ε on the *COP* can be investigated numerically. Because T_c and T_h are functions of various parameters as shown in Eq. (26), the *COP* defined in Eq. (29) represents nonlinear behaviors depending on not only the geometric parameters but also the physical properties of the materials as mentioned below in next section.

4. Results and discussion

To find the optimum conditions for maximizing the *COP* of TEC, the effect of key parameters on the *COP* is studied with the above procedure. The thermoelectric properties and TEC geometries used in the numerical calculation are summarized in Table 1.

The effect of γ (A_i/A_{TE}) on the *COP* is presented in Fig. 5. As can be seen, the *COP* increases rapidly to the maximum and then decreases slowly with γ. The results show that the enhancement of the *COP* goes up to 44% at $\gamma = 28$ (28, 0.59) and 42% at $\gamma = 10$ (10, 0.58) compared to $\gamma = 0$ (0, 0.41) where (A, B) denotes (γ-value, *COP*-value) as shown in Fig. 6. From the practical viewpoint, the optimum value of γ can be determined at about 10. In the production of convectional TEC, γ is also selected at about 10.

Table 1
Data used in calculation

Operating conditions		Geometries		Thermoelectricities	
T_{ho} (K)	313	A_{TE} (m^2)	0.0016	K_{TE} (W/K)	16
		A_i (m^2)	0.01	R (Ω)	5×10^{-3}
T_{co} (K)	273	d (m)	0.004	S (V/K)	5×10^{-4}
		σ_h	10	k_h, k_c (W/mK)	100
I (A)	2	σ_c	11	k_i (W/mK)	0.001
		ε	5	Zm	3.125×10^{-5}

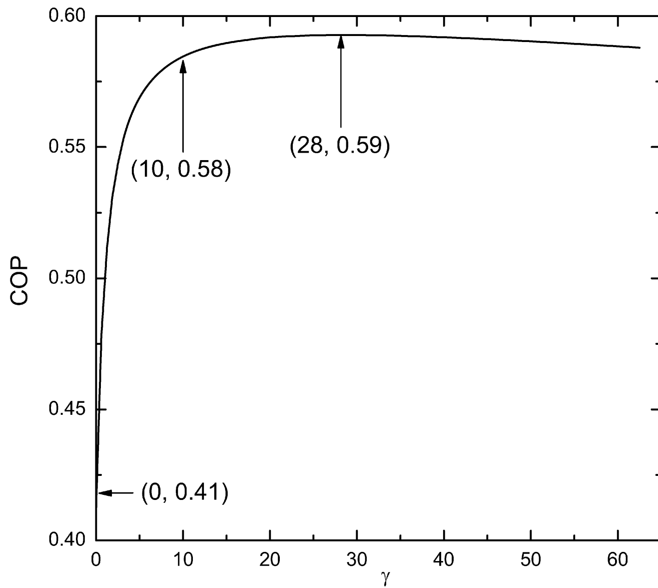

Fig. 5. The effect of γ $(= A_i/A_{TE})$ on the *COP* with given conditions in Table 1.

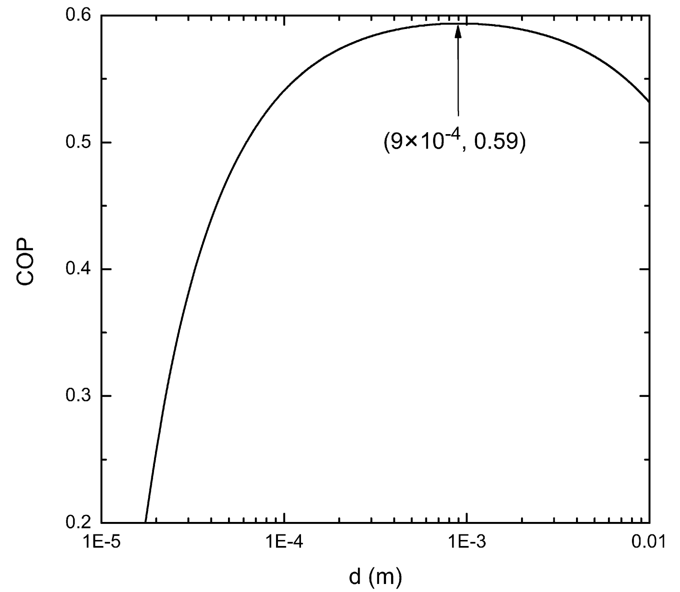

Fig. 7. The effect of TEM depth d on the *COP* with given conditions in Table 1.

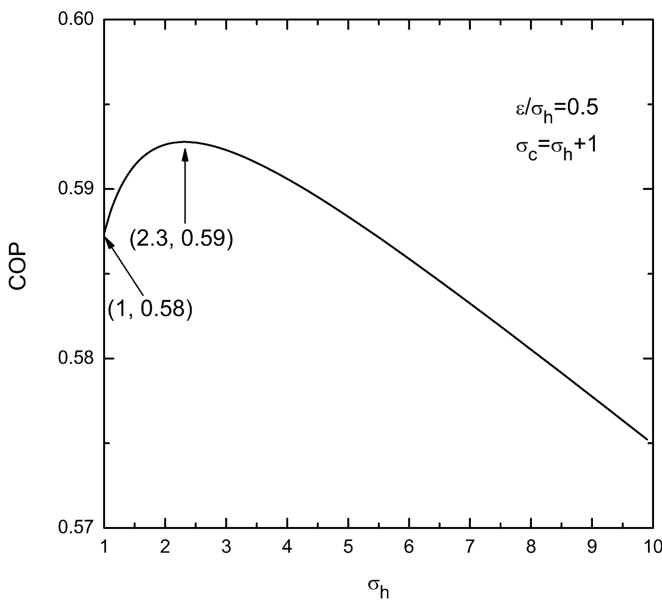

Fig. 6. The effect of σ_h on the *COP* with given conditions in Table 1.

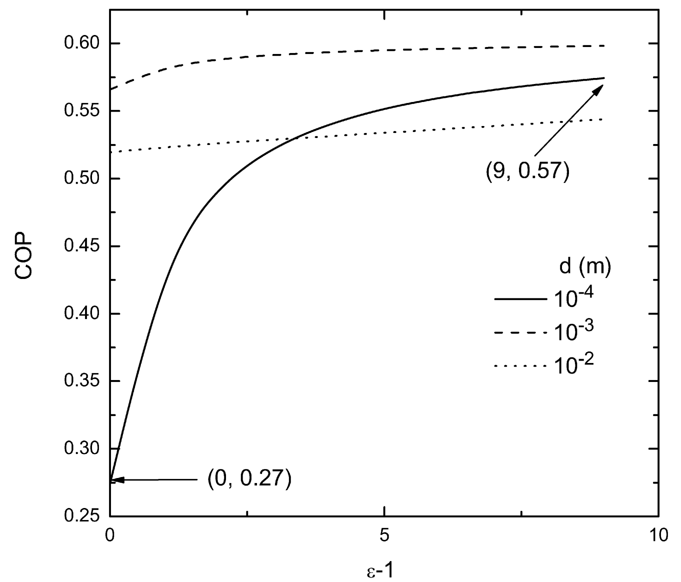

Fig. 8. Curves of the *COP* vs. $\varepsilon - 1$ for various TEM depth d with given conditions in Table 1.

Fig. 6 presents the effect of the ratio of heat sink depth to TEM one, σ_h on the *COP*. The results are obtained under the approximation that the depth of the spacer is a half of that of heat sink. The results show that the *COP* goes up to the maximum with respect to σ_h and then slows down. The reason can be given as follow: with decreasing σ_h, the depth of the spacer decreases linearly but the heat loss through the insulator increases exponentially. On the other hand, with increasing σ_h, the thermal resistance of heat sink increases exponentially. Therefore an optimum *COP* exists.

As illustrated in Fig. 7, the TEM depth, d significantly affects the *COP* of the TEC. It represents that the *COP* has the maximum at $d = 9 \times 10^{-4}$ m. The *COP* drops rapidly by heat loss with a decrease of d. Therefore, it is concluded that for the micro-TEC the reduction of heat loss is very important and the proper selection of the optimal TEM depth is inevitable. It has the same tendency as Min and Rowe's results [8].

Fig. 8 represents the *COP* versus the ratio of the spacer depth to the TEM one, $\varepsilon - 1$ for various d. As can be seen, the spacer has little effect on the *COP* for the case of TEM depths larger than 1.0 mm. However, in case of smaller than 1.0 mm ($d = 100$ μm), the *COP* is enhanced up to about 110% with the spacer of which the depth ratio, $\varepsilon - 1$ is 10 ($COP = 0.57$) compared to the *COP* without the spacer ($COP = 0.27$). Consequently, not only the selection of the TEM depth but also the insertion of the spacer is an important factor to enhance the *COP* in the design of a TEC.

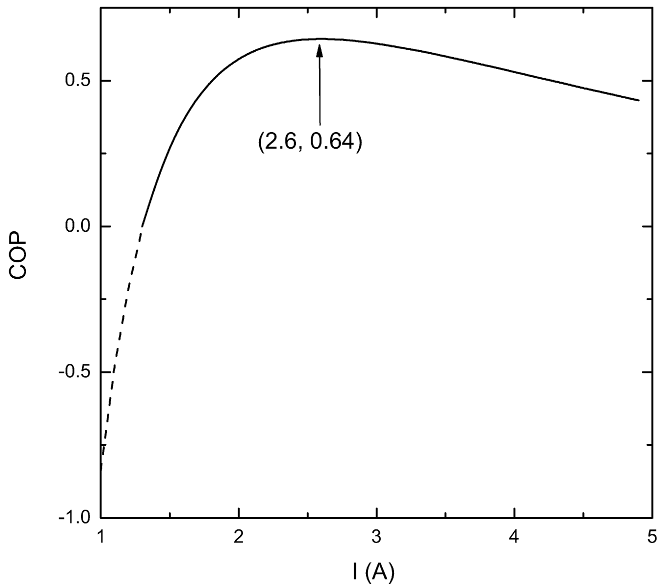

Fig. 9. The effect of current I on the COP with given conditions in Table 1.

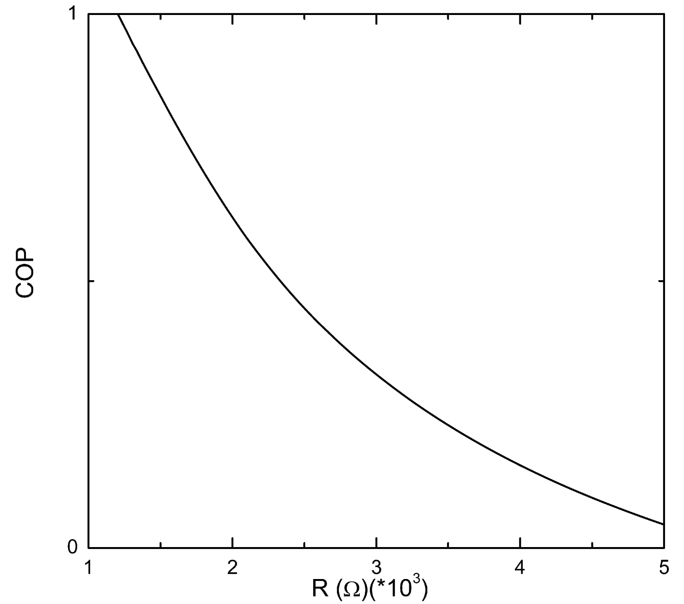

Fig. 11. The effect of R on the COP with given conditions in Table 2.

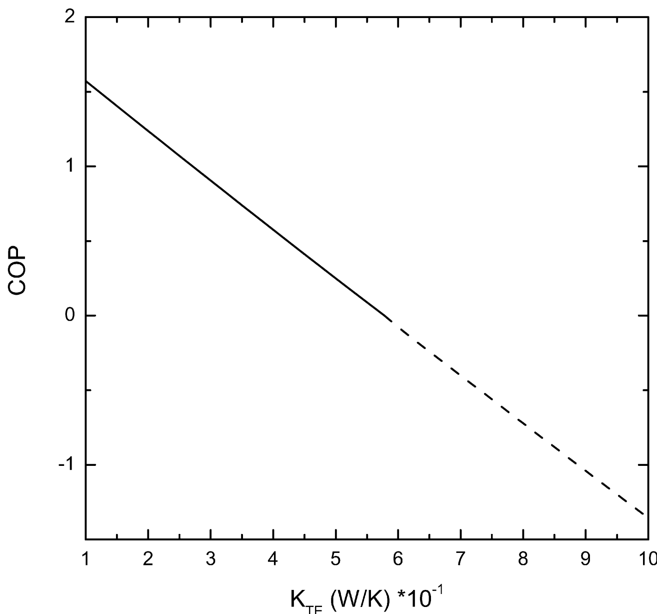

Fig. 10. The effect of K_{TE} on the COP with given conditions in Table 2.

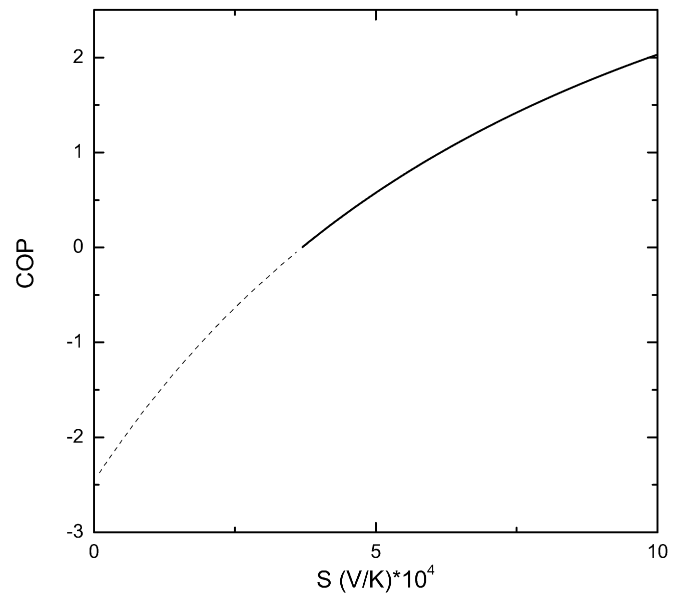

Fig. 12. The effect of S on the COP with given conditions in Table 2.

The current I, which is an operating condition for TEC, has a great influence on the COP, as shown in Fig. 9. These results have the same tendency as the previous studies [9,20], showing that there is an optimal value of current I. For the current I smaller than 0.5 A, the COP becomes negative. It means that the performance of the TEM for a cooling deteriorates with decreasing the current, and the direction of the heat transfer is finally switched between inside and outside of the TEC due to the lack of the electric power. It is presented with the dot line in Fig. 9.

The effect of thermoelectric properties such as K_{TE}, R and S on the COP is presented in Figs. 10–12, respectively. These results show that the COP rapidly increases with decreasing K_{TE} and R and with increasing S. It means that thermoelectric properties of materials are the key factors to enhance the COP.

Recently, the development of thermoelectric materials to improve the thermoelectricity is realized by using nanotechnology and pressure methods [6,21]. The performance of TEC and TEM is measured by figure of merit, Zm, defined as

$$Zm = \frac{S^2}{RK_{TE}} \tag{30}$$

The COP was expressed implicitly as a function of Zm and other dimensionless variables by Yamanashi [7]. In order to present explicitly the effect of thermoelectric properties such as S, R, and K_{TE} on the COP, we performed the calculation for four different pairs, (S, R, K_{TE}) with a given Zm. The result-

Table 2
Conditions of calculation and the critical values

Case	S (V/K)	R (Ω)	K_{TE} (W/K)	Zm (K^{-1})	Optimal I (A)	Maximum COP
A	2×10^{-4}	5×10^{-3}	4	2.0×10^{-5}	1.5	0.331
B	4×10^{-4}	1×10^{-2}	8	2.0×10^{-5}	1.5	0.327
C	2×10^{-4}	2.5×10^{-3}	8	2.0×10^{-5}	3.1	0.327
D	4×10^{-4}	5×10^{-3}	16	2.0×10^{-5}	3.1	0.316

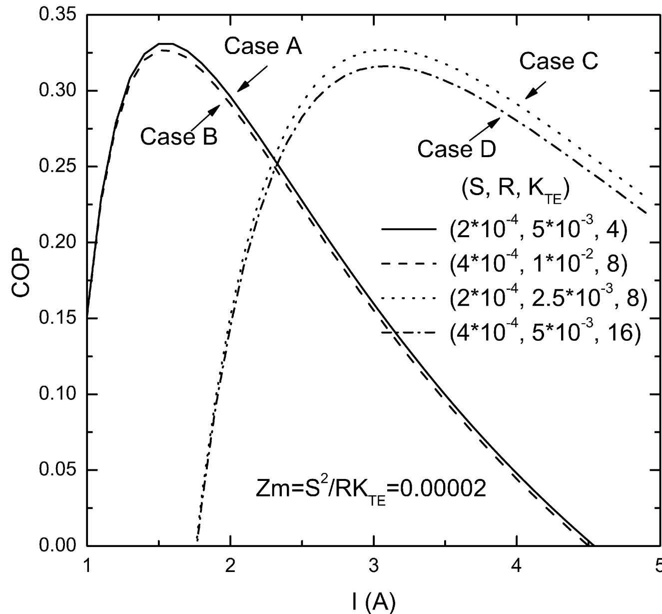

Fig. 13. Curves of the COP vs. I for various (S, R, K_{TE})-set with the same Zm.

ing curves of the COP with respect to the operating condition I are plotted in Fig. 13. As can be seen, graphs of case A and B are almost the same and those of case C and D change with respect to I. The calculation conditions and the critical values are summarized in Table 2, respectively. The thermal conductivity of the thermoelectric materials can be obtained based on the definition of the thermal conductance, K_{TE}, which is generally order of 1.0 W/m K. The results show that while the optimal I of cases A and B, and cases C and D are identical respectively, the maximum values of the COP are different depending on the combination of S, R, and K_{TE} (see Table 2). Therefore, it could be concluded that the combination pair of thermoelectric properties as well as Zm has to be taken into account for the selection of new thermoelectric materials. Bi2Te3, Re6Te15 and PbTe are commonly used as the materials of thermoelectric module. Based on the present results, a new material is to be selected with the optimum conditions of S, K_{TE} and R to obtain a maximum COP.

5. Conclusions

In the present study, the effect of key parameters on the COP of a TEC with spacer has been investigated theoretically. From the present study, the following conclusions are drawn.

1. From the unsteady, one-dimensional analysis of heat conduction, the symmetry profiles at cold, hot sides and insulator are obtained, and a dimensionless time to reach the steady state is determined, which can be practically adopted to reduce the start-up period during the operation of a TEM.
2. There is an optimum geometric condition for the TEC design. The COP is enhanced up to 44% at the optimal γ.
3. For micro-TEC, the COP is significantly affected by the TEM depth and spacer. Especially in the case of TEM depth of 100 μm, the COP is enhanced up to 110% at an optimal spacer depth ratio ($\varepsilon - 1$) of 10.
4. The combination pair of thermoelectric properties as well as Zm should be taken into account significantly for the development of new thermoelectric materials and for the optimum design of TEC.

It is expected that the results from the present study provide a guideline to design the TEC and the strategy to the development of thermoelectric materials.

Acknowledgements

The authors deeply appreciate the financial support provided by Korea Energy Management Corporation Grant (2004-E-NC03-P-02-0-000-2005), and MOCIE through EIRC program. The authors thank Mr. Chan Hyoung Park or his technical assistance for the present study.

References

[1] S.B. Riffat, X. Ma, Thermoelectrics: a review of present and potential applications, Applied Thermal Engineering 23 (2003) 913–935.
[2] H. Hasegawa, K. Sato, H. Okumura, K. Nakamura, S. Yamaguchi, K. Miyake, Reduction of heat leak in cryogenic system using Peltier current leads, Cryogenics 42 (2002) 495–500.
[3] N.F. Güler, R. Ahiska, Design and testing of a microprocessor-controlled portable thermoelectric medical cooling kit, Applied Thermal Engineering 22 (2002) 1271–1276.
[4] R. Venkatasubramanian, E. Silvola, T. Colpitts, B. O'Quinn, Thin-film thermoelectric devices with high room-temperature figures of merit, Nature 413 (2001) 579–602.
[5] F. DiSalvo, Thermoelectric cooling and power generation, Science 285 (1999) 703–706.
[6] M.S. Toprak, Engineered nanostructures and thermoelectric nanomaterials, PhD thesis, Royal Institute of Technology, Stockholm, Sweden, 2003.
[7] M. Yamanashi, A new approach to optimum design in thermoelectric cooling system, Journal of Applied Physics 80 (1996) 5494–5502.
[8] G. Min, D.M. Rowe, Cooling performance of integrated thermoelectric microcooler, Solid-State Electronics 43 (1999) 923–929.
[9] B.J. Huang, C.J. Chin, C.L. Duang, A design method of thermoelectric cooler, International Journal of Refrigeration 23 (2000) 208–218.
[10] J. Luo, L. Chen, F. Sun, C. Wu, Optimum allocation of heat transfer surface area for cooling load and COP optimization of a thermoelectric refrigerator, Energy Conversion and Management 43 (2003) 3197–3206.

[11] Y.H. Cheng, C. Shih, Maximizing the cooling capacity and COP of two-stage thermoelectric coolers through genetic algorithm, Applied Thermal Engineering 26 (2006) 937–947.
[12] J. Yu, H. Zhao, K. Xie, Analysis of optimum configuration of two-stage thermoelectric modules, Cryogenics (2006), doi:10.1016/j.cryogenics.2006.09.010.
[13] A. Chakraborty, K.C. Ng, Thermodynamic formulation of temperature-entropy diagram for the transient operation of a pulsed thermoelectric cooler, International Journal of Heat and Mass Transfer 49 (2006) 1845–1850.
[14] A.K. Pramanick, P.K. Das, Constructal design of a thermoelectric device, International Journal of Heat and Mass Transfer 49 (2006) 1420–1429.
[15] L.N. Vikhor, L.I. Anatychuk, Theoretical evaluation of maximum temperature difference in segmented thermoelectric coolers, Applied Thermal Engineering 26 (2006) 1692–1696.
[16] K. Chen, S.B. Gwilliam, An analysis of the heat transfer rate and efficiency of TE (thermoelectric) cooling system, International Journal of Energy Research 20 (1996) 399–417.
[17] H.S. Carslaw, J.C. Jager, Conduction of Heat in Solids, second ed., Oxford Univ. Press, London, 1959, pp. 309–310.
[18] T.C. Harman, J.M. Honig, Thermoelectric and Thermomagnetic Effects and Applications, McGraw–Hill Book Company, New York, 1967.
[19] H.J. Goldsmid, Conversion efficiency and figure-of-merit, in: D.M. Rowe (Ed.), CRC Handbook of Thermoelectrics, CRC Press, London, 1995, pp. 27–42.
[20] Y.J. Dai, W.L. Li, Experimental investigation and analysis on a thermoelectric refrigerator driven by solar cells, Solar Energy Materials & Solar Cells 77 (2003) 377–391.
[21] J.F. Meng, N.V. ChandraShekar, D.Y. Chung, M. Kanatzidis, J.V. Badding, Improvement in the thermoelectric properties of pressure-tuned β-$K_2Bi_8Se_{13}$, Journal of Applied Physics 94 (2003) 4485–4488.